ASTRO-H

INSTRUMENT CALIBRATION REPORT
SXS RESPONSE MATRIX
ASTH-SXS-CALDB-RMFPARAM

Version 2.0

DATE December 14th 2016

ISAS/ GSFC

Prepared by: Maurice Leutenegger, Meng Chiao, Megan Eckart, Rich Kelley, Caroline Kilbourne, Scott Porter, Tomomi Watanabe

Table of Contents

CHANGE RECORD PAGE (1 of 2)

DOCUMENT TITLE : SXS Response Matrix			
ISSUE	DATE	PAGES AFFECTED	DESCRIPTION
Version 1.0	August 22nd 2016	All	First on-orbit
Version 2.0	December 14th 2016		Physical model for extended LSF

1 Introduction

1.1 Purpose

This document describes how the response matrix file (RMF) is calculated and how the parameters defined in the CALDB file were derived. The RMF is a matrix which describes the distribution of measured photon energies for incident monochromatic input photons.

The response is characterized by two conceptually different parts to the line spread function (LSF): a Gaussian core LSF, and an extended LSF due to several different physical mechanisms. Each pixel and event grade has its own core LSF, and the core LSF may change over time if the SXS noise environment changes, and if the event templates are changed. The extended LSF is the same for all pixels and event grades, and is not expected to change.

1.2 Scientific Impact

The core LSF and extended LSF parameters are used by `sxsrmf` to calculate pixel-by-pixel RMFs.

2 Release CALDB 20161122

Filename	Valid data	Release date	CALDB Vrs	Comments
ah_sxs_rmfparam_20140101v003.fits	2014-01-01	20161122	005	sxs_rmf_extended_0.5.1.fits

2.1 Data Description

This update is based on more complete physical modeling of ground calibration data described in Release 20160310.

2.2 Data Analysis

Ground calibration data for additional monochromator energies were analyzed to obtain additional constraints on the electron loss continuum and escape peak strengths. These constraints should be considered preliminary, and may suffer from significant systematic errors due to limitations in the rigor of the data analysis procedures.

2.3 Results

We implemented a new physical model to calculate the strengths of the electron loss continuum and escape peaks from first principles.

For each escape peak, the strength relative to the main peak is given as follows. The escape probability as a function of penetration depth z and fluorescent energy E_f can be calculated by integrating the absorber optical depth at E_f along a ray through the absorber over the uniform angular probability of emission. This can then be integrated over penetration depth for the incoming photon energy E_i to obtain the penetration depth averaged escape probability. The averaged escape probability is then multiplied by the fractional probability of creating the appropriate inner shell vacancy which is the parent state corresponding to the fluorescent line in question; and by the fluorescent yield for that vacancy; and finally by the branching ratio for fluorescence to the given line.

The fluorescence data are obtained from the complilation of Crawford et al. 2011 (ANSTO/E-744). The fractional probability of creation of the appropriate inner shell vacancy is calculated using total photoionization cross sections from Henke et al. (1993) and subshell photoionization cross sections from FAC atomic calculations (Gu 2004). The escape probabilities were calculated using the same total photoionization cross sections from Henke et al. In Figures 1 and 2 we compare measurements of the strongest escape peaks to the strengths predicted by the model.

The electron loss continuum is calculated using the same method to determine the penetration depth of the incoming photon and the probability of obtaining a given core vacancy. The photoelectron then has known energy based on the incoming photon energy and the binding energy of the inner shell electron. The Auger spectrum is approximated by assuming that the remaining energy is assigned to a single Auger electron, with a production efficiency equal to unity minus the fluorescence efficiency.

The loss of energy by electrons propagating in the absorber was assumed to follow the empirically derived relation of Iskef et al. (1983). We derived a method to calculate the full electron loss spectrum for a monochromatic input photon energy by integrating over propagation angle of photo- and Auger electrons, and by integrating that over penetration depth of the incoming photon. However, because of the design decision in sxsrmf to approximate the spectrum of the electron loss continuum as flat in counts per unit energy bin, it is not necessary to calculate the full electron loss spectrum. We can instead simply calculate the probability of an electron escaping and integrate this over the penetration depth of the incoming photon. This is averaged over the spectrum of photo- and Auger electrons for a given vacancy. Finally, this is multiplied by the vacancy probability, and the spectra for all vacancies are summed. In Figure 3, we compare the predicted electron loss continuum fraction with measurements from the ground calibration data.

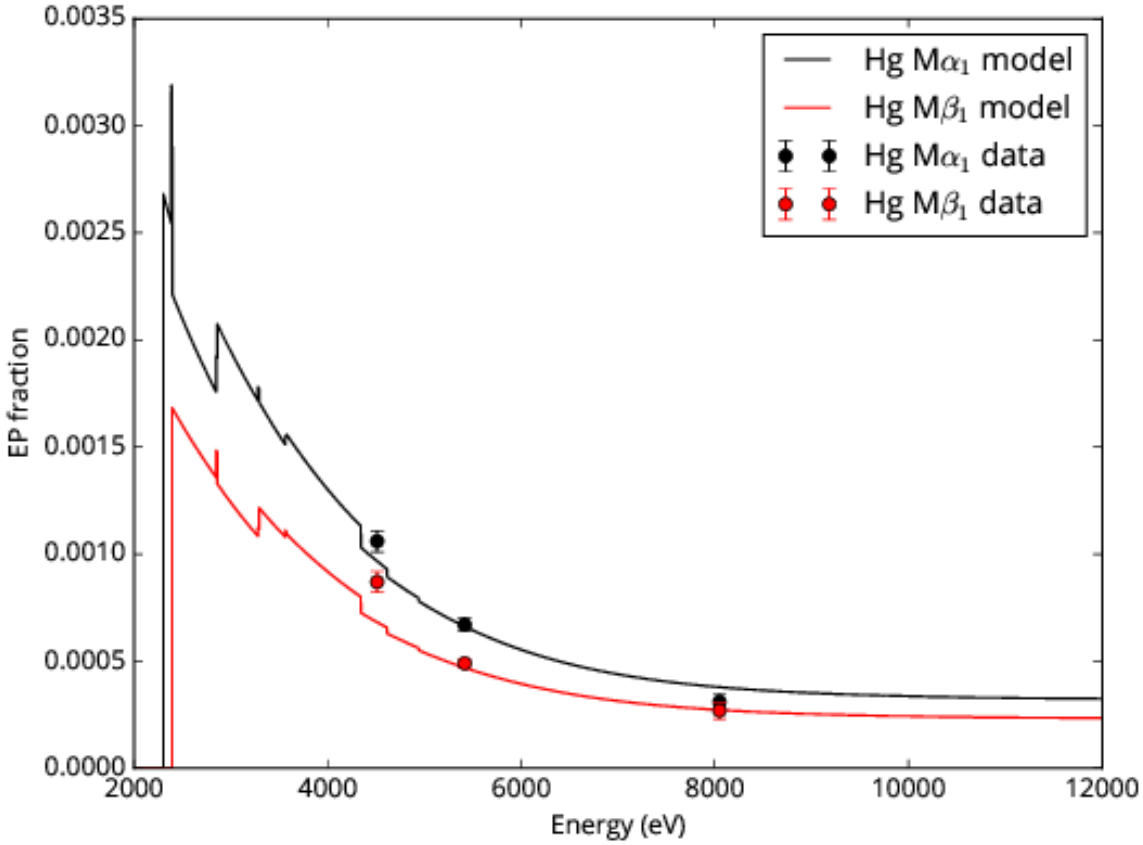

Figure 1. Fraction of events in strongest Hg M escape peaks as a function of incoming photon energy. Data points are from ground calibration experiments. Solid lines are models. An example of a data set showing escape peaks can be seen in Figure 9.

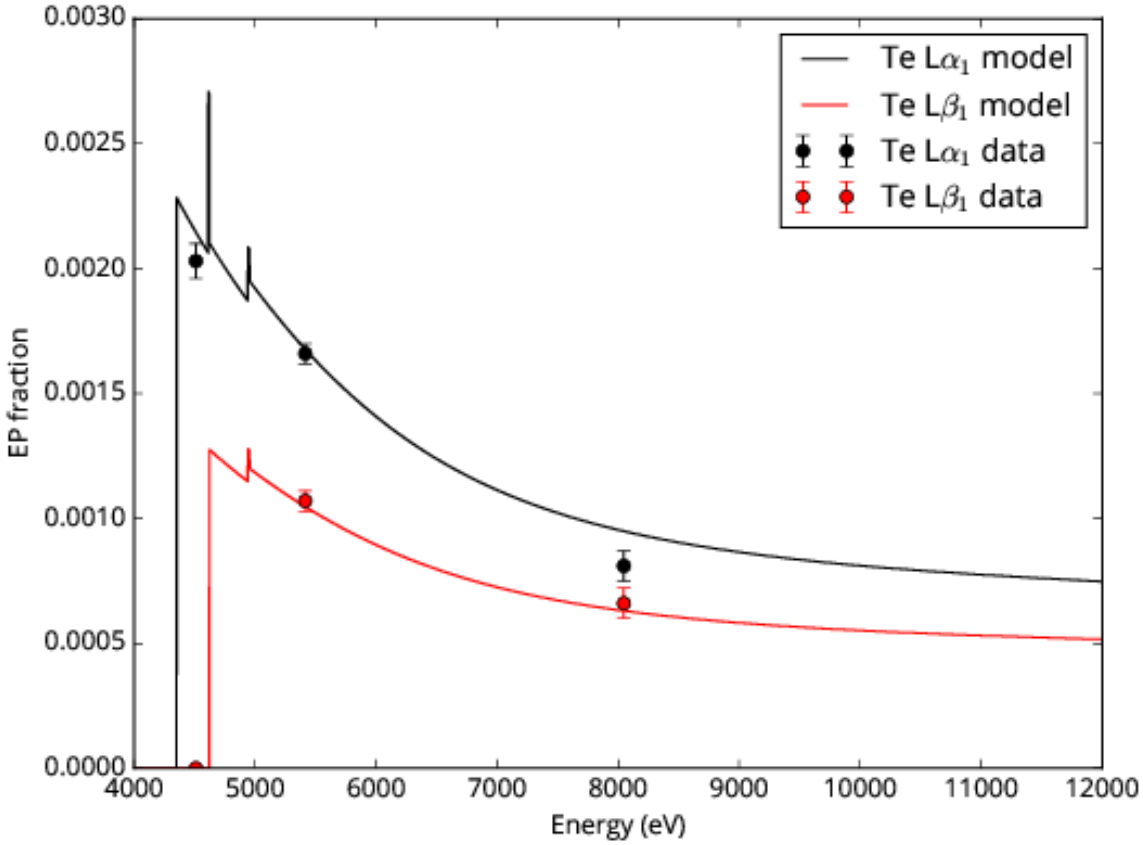

Figure 2. Fraction of events in strongest Te L escape peaks as a function of incoming photon energy. Data points are from ground calibration experiments. Solid lines are models. An example of a data set showing escape peaks can be seen in Figure 9.

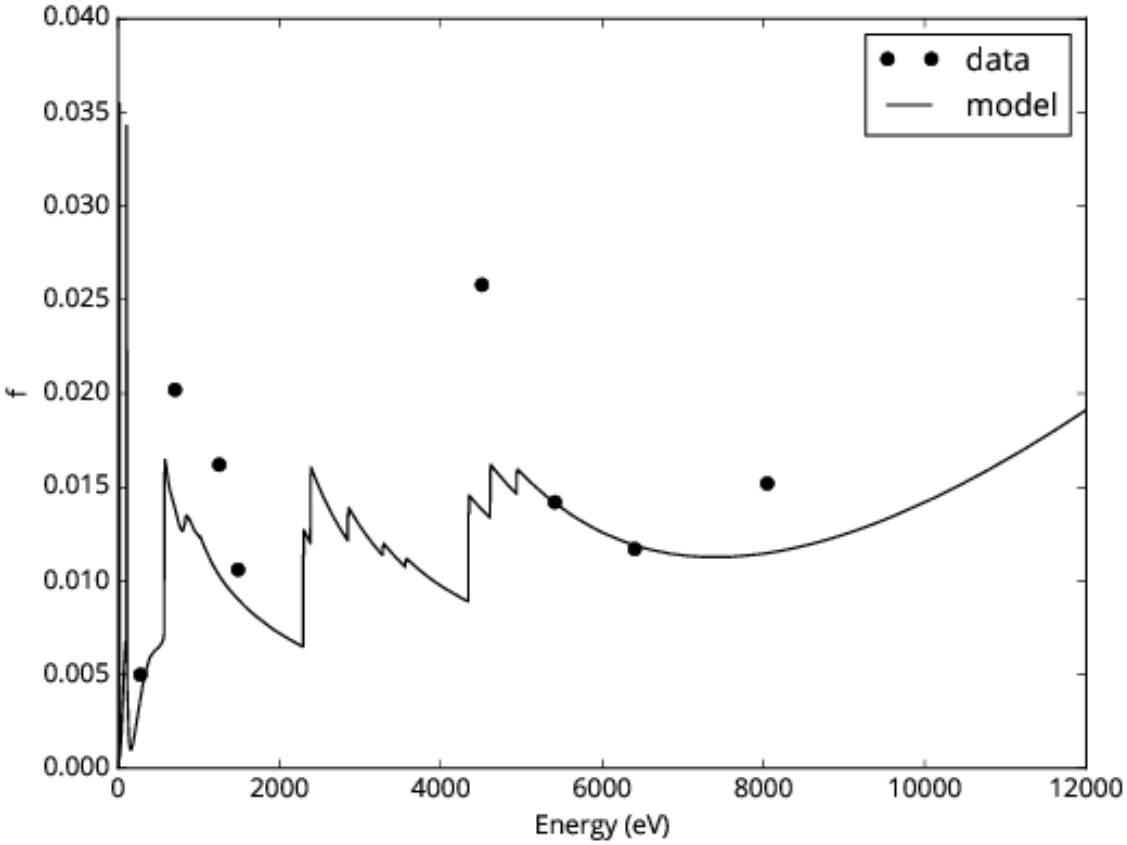

Figure 3. Fraction of events in the electron loss continuum as a function of incoming photon energy. Data points are from ground calibration experiments. The solid line is the model.

2.4 Comparison to last release

This is the first release of extended LSF products which uses a physically motivated model for the electron loss continuum and escape peaks instead of a placeholder. It still contains significant approximations, most notably: 1. The electron loss continuum shape is still assumed to be flat in counts per unit energy bin; and 2. The shape of escape peak fluorescent lines is not taken into account, and non-diagram lines are lumped in with their corresponding parent diagram lines. Given that the main impact of the extended LSF is in modeling redistribution of the continuum, even in the relatively line-rich spectrum of Perseus, these approximations are acceptable.

The model for the exponential tail has not changed, and is empirically motivated but not explicitly modeled.

The core LSF has not been updated.

2.5 Bibliography

Crawford et al. 2011 ANSTO/E-774
Henke et al. 1993 ADNDT 54 181
Gu 2004 AIP Conf. Proc. 730 127
Iskef et al. 1983 Phys. Med. Biol. 28 535

3 Release CALDB 20160606

Filename	Valid data	Release data	CALDB Vrs	Comments
ah_sxs_rmfparam_20140101v002.fits	2014-01-01	20160606	003	Derived from file sxs_rmf_FWHM_0.3.2.fits

3.1 Data Description

The data supplied in this update were obtained using the ^{55}Fe filter wheel exposure experiment.

3.2 Data Analysis

The data were analyzed to obtain the following parameters: FWHM resolution for hires and midres primary events at 5.9 keV; resolution for lowres primary events by analysis of lowres raw pulseheight for hires events; and resolution for (hires) baselines.

3.3 Results

The measured baseline resolution was slightly higher than in the instrument level calibration tests performed at TKSC in March 2015. Assuming the same excess broadening, one can predict the resolution as a function of energy. The measured resolution at 5.9 keV is statistically consistent with this prediction, with the exception of Pixel 12, which has slightly increased excess broadening. We therefore model the on-orbit resolution using the pre-flight excess broadening combined with the on-orbit baseline resolution.

There were many fewer midres events, and no midres baselines. We did find that the midres resolution was statistically slightly higher than in pre-flight measurements, leading to the conclusion that midres primaries also likely have the same excess broadening as in pre-flight measurements. We estimated the midres baseline resolution to be higher in proportion to the hires baseline resolution by a factor of 1.087. We then followed the same procedure, using the pre-flight excess broadening combined with the estimated on-orbit baseline resolution.

We did not analyze the lowres raw pulseheights of the baselines, so we simply scaled up the pre-flight lowres primary resolution curve to match the on-orbit measured values.

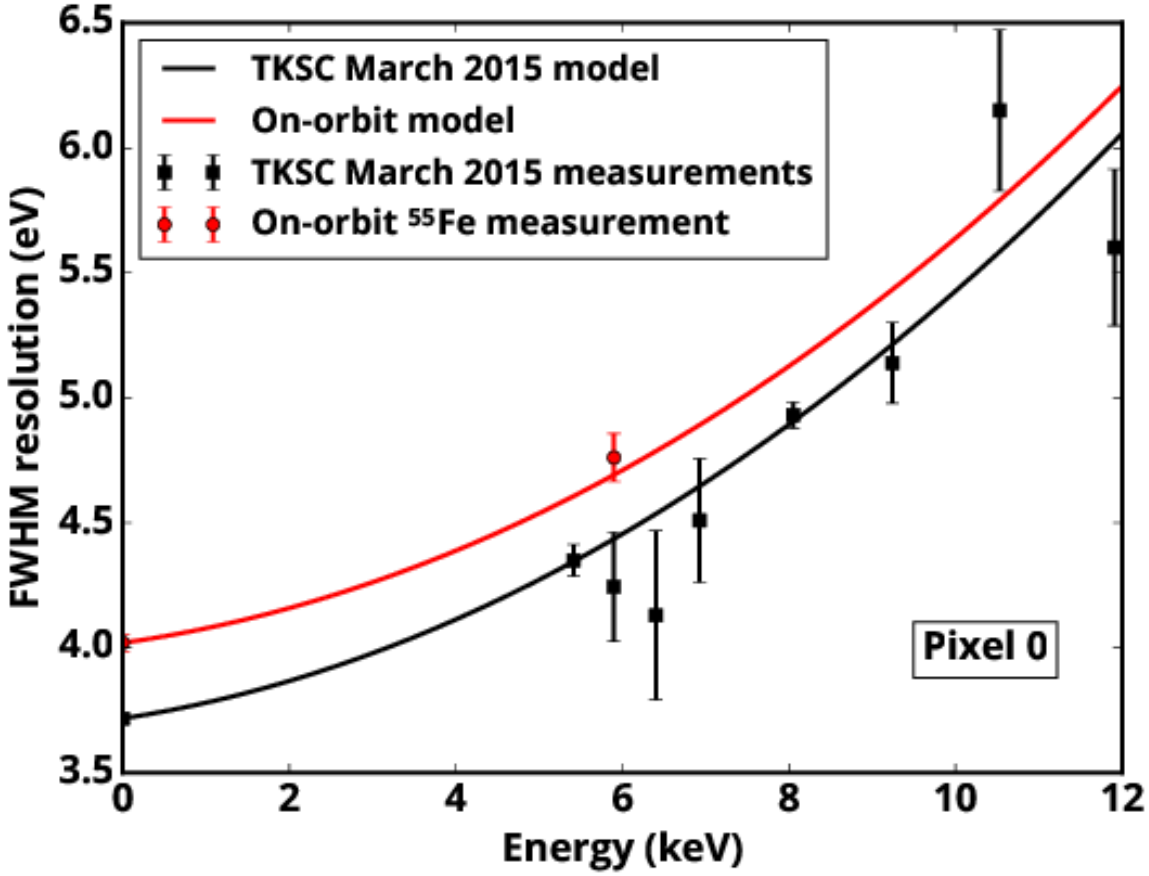

Figure 4. Resolution for hires events on pixel 0 (as in Figure 2), updated for on-orbit measurements of the baseline and 5.9 keV resolution.

3.4 Comparison to last release

The core LSF has been updated to reflect on orbit performance. There is no update to the exponential tail, electron loss continuum, or escape peaks. These parameters are still placeholders.

4 Release CALDB 20160310

Filename	Valid data	Release data	CALDB Vrs	Comments
ah_sxs_rmfparam_20140101v001.fits	2014-01-01	20160310	001	Derived from file sxs_rmf_FWHM_0.2.2.fits; sxs_rmf_extended_0.1.fits

4.1 Data Description

4.1.1 Core LSF

The core LSF in this release is based on the LSF measured in the final flight configuration in instrument level testing in TKSC in March 2015. These experiments used flight electronics boxes, including the ADR controller (ADRC), detector analog readout electronics (Xbox), and digital pulse shape processor (PSP).

In one set of experiments, the detector was illuminated by a channel cut crystal monochromator (CCCM) in two configurations giving monochromatized photons from electron impact sources producing Cu $K\alpha_1$ and Cr $K\alpha_1$. In another set of experiments, the detector was illuminated by the rotating target source (RTS), in which photons from an electron impact source fluoresce targets mounted on a rotatable wheel. The target materials used in these experiments are Fe, KBr, Cu, GaAs, Co, Cr, Mn, and TiO_2. Of these, Cr, Cu, and TiO_2 were not used for LSF calibration: the Cr and Cu results were not as precise as those obtained with the CCCM, and the TiO_2 results suffered from systematic uncertainties in the model fluorescence line shape.

All of the data used to measure the core LSF was acquired using SHPTEMPL=2015-03-10.

Experiment filename	**Start time (UT)**	**Stop time (UT)**	**type**	**notes**
15-03-13.10.24.35Z.pxp	3509087083.58	3509111046.09	Cu CCCM	
15-03-12.06.28.11Z.pxp	3508986495.26	3508997317.02	Cr CCCM	Partial coverage
15-03-12.09.57.19Z.pxp	3508999037.82	3509009955.04	Cr CCCM	Partial coverage
15-03-11.16.24.16Z.pxp	2015-03-11 16:25	2015-03-12 04:38	RTS	
15-03-12.13.56.25Z.pxp	2015-03-12 13:59	2015-03-13 01:08	RTS	Forced midres

Table 1 Log of experiments used to measured core LSF

Element	**Energy (eV)**	
	$K\alpha_1$	$K\alpha_2$
Cr	5414.7	5405.5
Mn	5898.8	5887.6
Fe	6403.8	6390.8
Co	6930.3	6915.3
Cu	8047.8	8027.8
Ga	9251.7	9224.8
As	10543.7	10508.0
Br	11924.2	11877.6

Table 2 Energies of lines used in RTS experiments.

4.1.2 Extended LSF

The electron loss continuum and exponential tail parameters are based on estimates derived from measurements in the GSFC Maggie Dewar using the SNR monochromator and CCCM

monochromator. The escape peak energies are from Kaye & Laby, and the intensities are estimates based on CCCM data.

Experiment filename	Start time (UT)	Stop time (UT)	Type/lines	notes
12-12-11.19.02.13.pxp			SNR/OK	
12-12-13.18.45.12.pxp			SNR/CK	
12-12-10.10.56.40.pxp			SNR/FeL	
12-11-24.15.51.01.pxp			SNR/MgK	
12-11-19.12.47.40.pxp			SNR/AlK	
13-01-18.13.13.12.pxp			CCCM/CuK	
12-11-11.22.17.43.pxp			CCCM/CrK	

Table 3 Log of experiments used for extended LSF; analysis is preliminary

4.2 Data Analysis

4.2.1 Core LSF

The core LSF was measured for each pixel and event grade for several different energies using custom fitting codes. CCCM data were fit with Gaussians, and RTS data were fit with literature fluorescent line shapes convolved with Gaussians. The core FWHM was tabulated as a function of energy for each pixel and event grade and this was fit with a 2^{nd} order polynomial.

4.2.2 Extended LSF

Since the energy loss mechanisms in the extended LSF apply to all event grades, data sets were filtered to use only hires events in order to simplify the analysis.
The electron loss continuum and exponential tail spectra were fit in Xspec using a custom model, with the fraction of counts in each as free parameters. This was measured for each of the SNR and CCCM data sets listed in the table.

The escape peak intensities were estimated for the CCCM data using Gaussian fits, and the relative intensities were obtained by normalizing to the core line.

4.3 Results

4.3.1 Core LSF

We find that the core LSF for a given pixel is Gaussian at any energy, down to at least three orders of magnitude from the peak at 5.4 keV, and to comparable levels at other energies, as illustrated in Figure 1. We have measured the width of the Gaussian as a function of energy for the FM DA as a subsystem in a test Dewar, as well as at the instrument level in the FM Dewar. This width will have to be recharacterized on orbit, since the different thermal and noise environments will provide different contributions to the LSF broadening budget.

Based on the instrument level measurements of lines produced by monochromators as well as of non-monochromatized fluorescence lines, which occurred in a roughly constant noise environment, we find that the core Gaussian FWHM energy resolution of each event grade for each pixel scales as a quadratic function of energy. An example is shown in Figure 2.

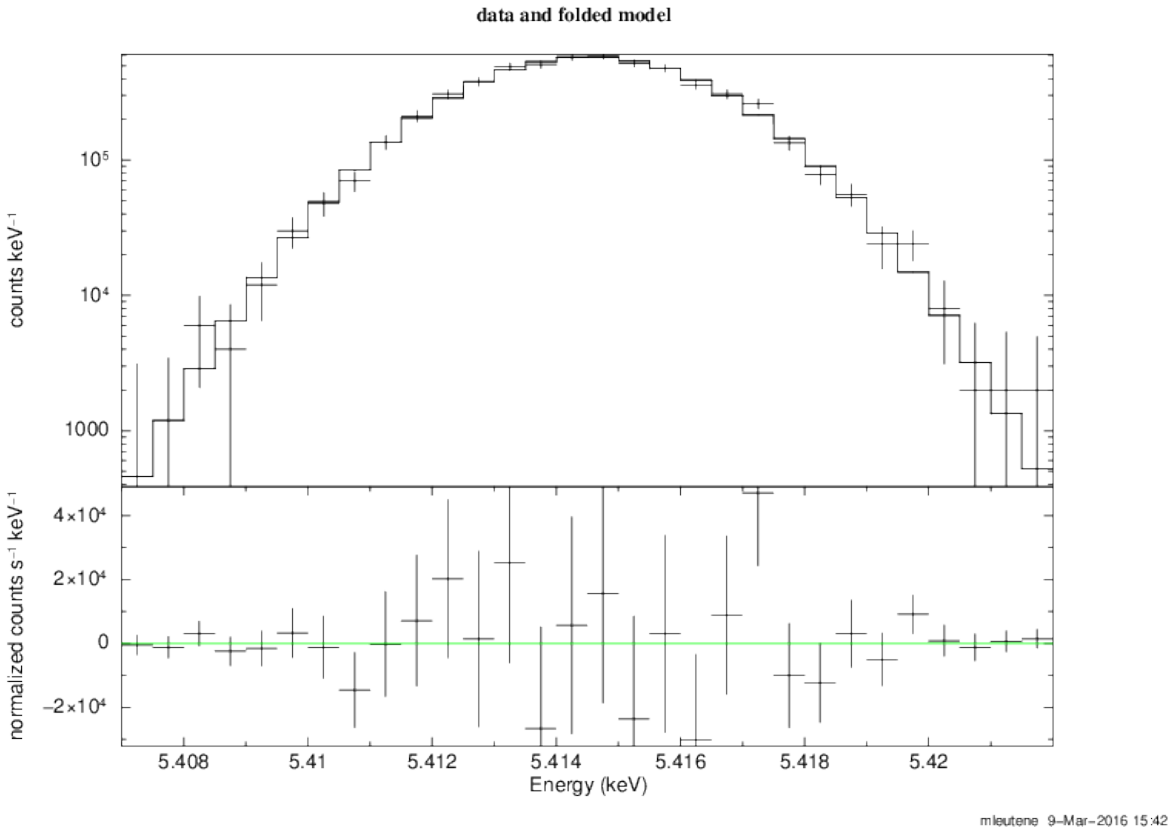

Figure 5.Gaussian fit to the observed spectrum of pixel 3 HR events from an experiment with a monochromator at 5415 eV. The FWHM of the monochromator is 0.24 eV.

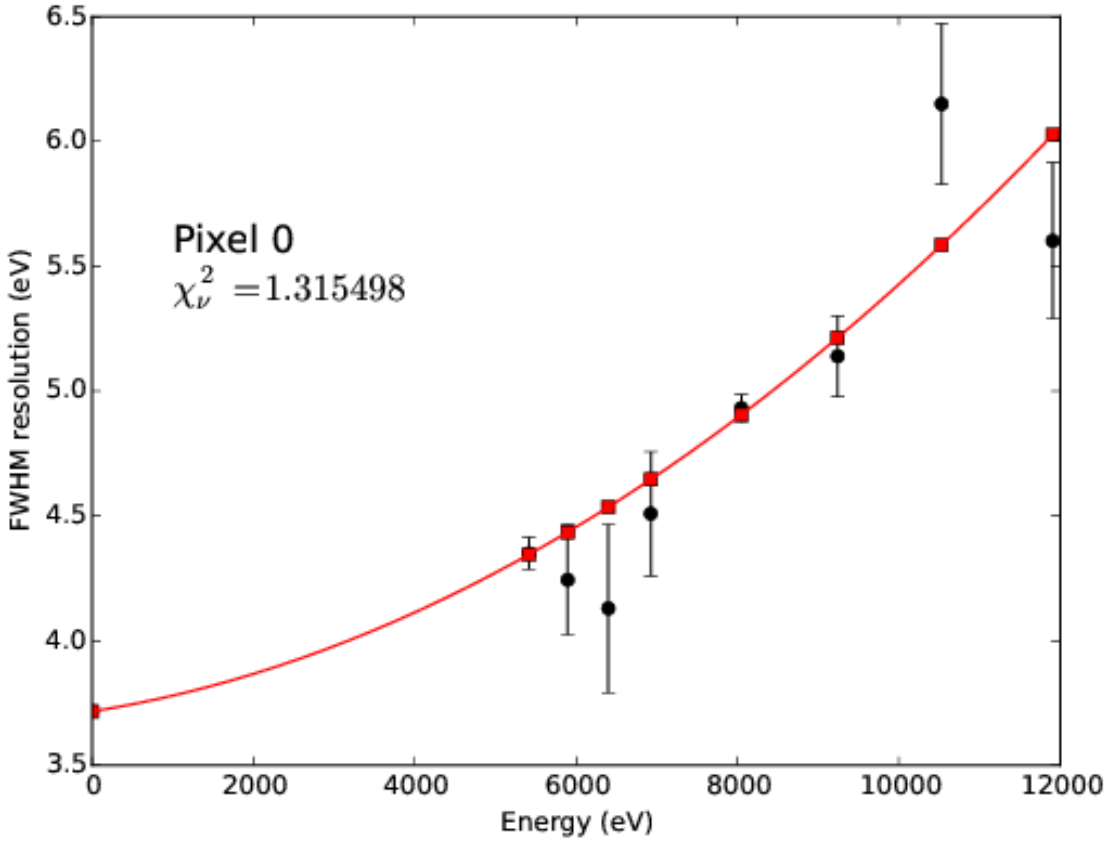

Figure 6. Measured and modeled FWHM resolution of HR events in Pixel 0. The measured points are from the calibration campaign in the FM Dewar in March 2015. The two data points with small error bars at 5415 eV and 8048 eV are from measurements with monochromators. The data point at 0 eV is from baseline events. The other data points are from deconvolution of fluorescence lines. The best-fit model is a quadratic function of energy.

4.3.2 Extended LSF

There are several energy loss mechanisms that result in a low energy tail in the RMF. These include long lived surface state excitations, giving rise to an exponential tail with e-folding of about 12 eV; scattering of primary or secondary photoelectrons out of the absorber, resulting in the so-called electron loss continuum, which is empirically found to have roughly constant flux per unit energy interval; and X-ray fluorescence photons which escape from the absorber instead of being thermalized, resulting in escape peaks.

An example of the redistribution of a low energy line is shown in Figure 3. The exponential tail with 12 eV e-folding is clearly visible. In Figure 4 we show the fraction of events falling in the exponential tail as a function of energy, as well as a calculation of the probability of a photon

stopping within a given distance of the absorber surface. The good agreement between the model and data shows that the probability of an event ending up in the tail is directly related to the penetration depth of the incident photon. This relation can be used to interpolate the fraction of events falling in the tail for other energies. Note that although this model reproduces the measured points reasonably well, it should be replaced by a more physically motivated model in the future.

Measurements of the electron loss continuum and escape peaks exist for several discrete input energies. The final calibration product requires a sophisticated model that can reproduce the measurements. Since this model is not yet complete, the parameters entered into the pre-flight CALDB files are placeholders, with values chosen to fall in the correct order of magnitude. Since the values are only placeholders, they should not be used for serious analysis.

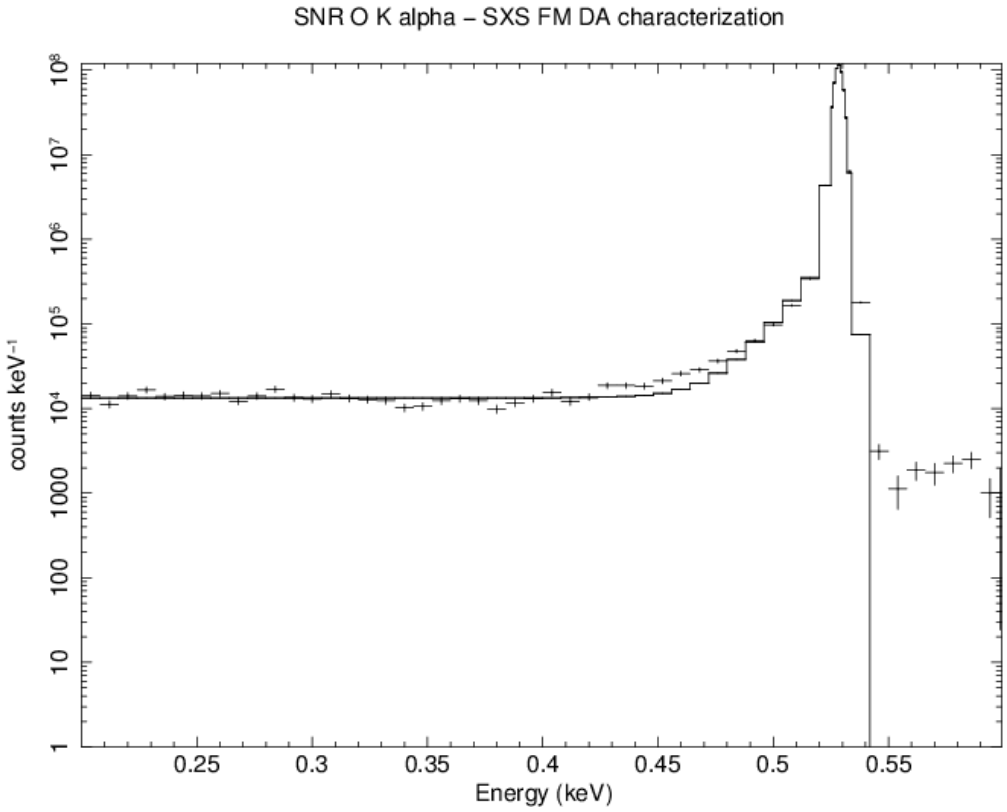

Figure 7 We show an example of a fit to data acquired with monochromatized O K shell fluorescence line emission in Figure 1. The core of the LSF is modeled with a Gaussian, and the tail is modeled with a flat (in energy) continuum to represent the electron loss continuum, and an exponential to represent energy lost to long-lived surface excitations. No significant escape peaks are present for incident photons with energies below the Hg M ionization threshold at 2295 eV. The tail on the high energy side of the line is an artifact of the monochromator.

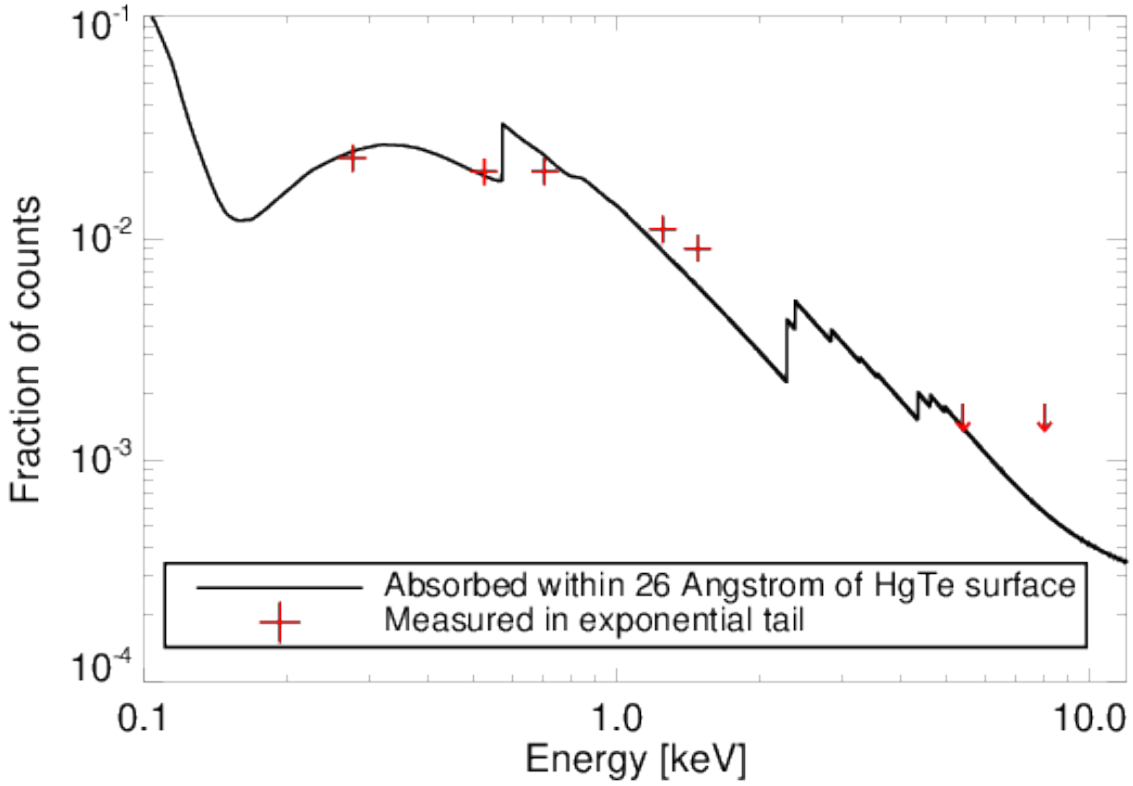

Figure 8 Absorption fraction as a function of photon energy in a surface layer on the HgTe absorbers (black solid line), plotted together with the fraction of events in the exponential tail (crosses).

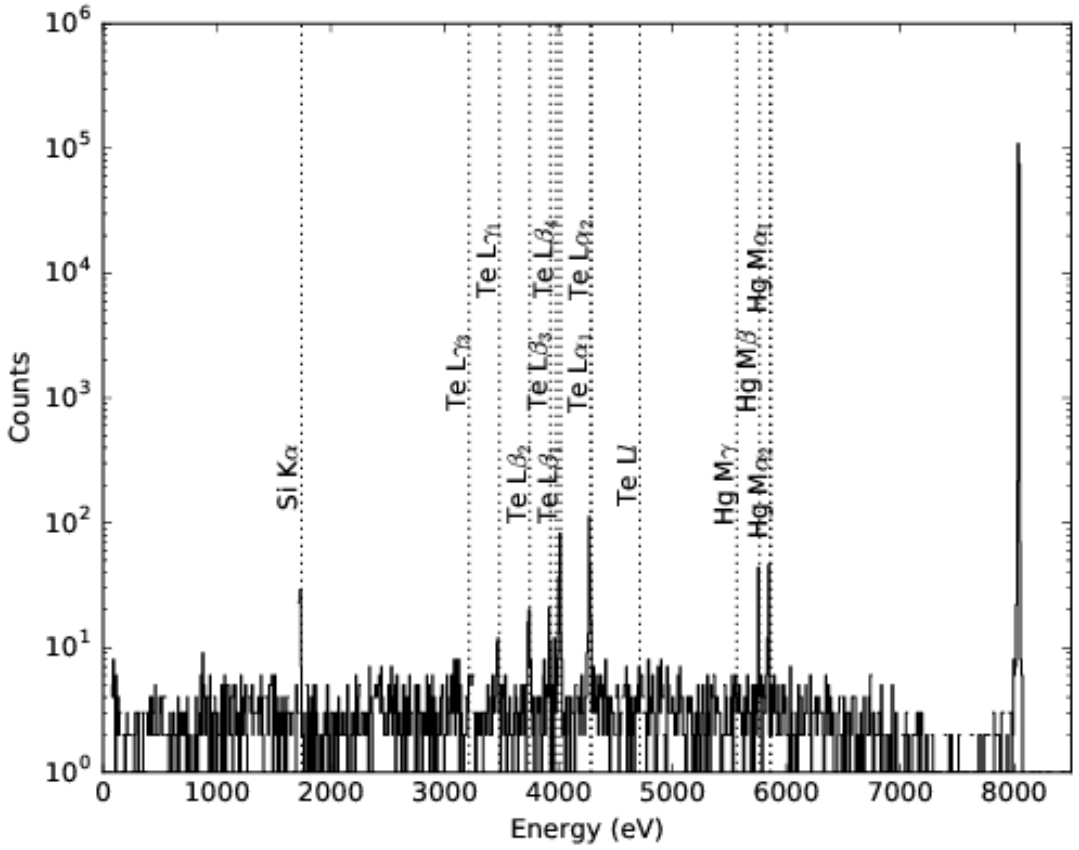

Figure 9 Spectrum acquired in SXS FM Dewar using Cu $K\alpha_1$ monochromator. Locations of Hg M and Te L escape peaks are marked. Si Kα fluorescence from the detector frame is also present.

4.4 Calibration products and response matrix parameters

We supply data products for the production of RMFs with different degrees of detail, depending on the needs of users. The four RMF categories are small (Gaussian only), medium (adds exponential tail), large (adds escape peaks), and extra-large (adds electron loss continuum).

The parameters for constructing these RMFs are contained in the file ah_sxs_rmfparam_YYYYMMDDvVVV.fits. The first extension, LINESIGMA, contains a description of the per-pixel, per-event-grade Gaussian FWHM broadening as a function of energy. The first column (ENERGY) is energy in eV, while each remaining column corresponds to a single pixel (PIXELN, 0<=N<=35). Each entry in these columns is an array of three FWHM resolutions in eV, corresponding to that for hires, midres primary, and lores primary events. The

parameters are defined on an energy grid extending from 10 eV to 40 keV in 0.25 eV bins. The values supplied above 12 keV are extrapolated and are thus likely to have significant errors.

The second extension, LINETAU, contains parameters that describe the exponential tail, escape peaks and electron loss continuum. These parameters are assumed to be the same for all pixels. The first column (ENERGY) is energy in eV. The exponential tail is characterized by two parameters, the e-folding energy in eV (TAU), and the fraction of events going to the tail (F_TAU). The electron loss continuum is characterized by a single parameter, the fraction of events going into it (F_ELC). The escape peaks comprise the remainder of the data in this extension. Each peak is described in the header with energy in eV (EPN, with 0<=N<=13), and label (LABEPN). The fraction of events going into each peak is given by F_EPN in the table extension.

4.5 Final remarks

This is the first documented release of this CALDB file based on ground measurements, and the final pre-launch release.

4.6 Bibliography

Kaye & Laby:

http://www.kayelaby.npl.co.uk/atomic_and_nuclear_physics/4_2/4_2_1.html